Nationaal Lucht- en Ruimtevaartlaboratorium

National Aerospace Laboratory NLR

NLR-TP-2012-332

Trailing edge noise: A benchmark for PIV based noise prediction

M. Tuinstra, S. Oerlemans and J.H.M. Gooden

Nationaal Lucht- en Ruimtevaartlaboratorium
National Aerospace Laboratory NLR

Anthony Fokkerweg 2
P.O. Box 90502
1006 BM Amsterdam
The Netherlands
Telephone +31 (0)88 511 31 13
Fax +31 (0)88 511 32 10
Web site: http://www.nlr.nl

Nationaal Lucht- en Ruimtevaartlaboratorium

National Aerospace Laboratory NLR

Executive summary

Trailing edge noise: A benchmark for PIV based noise prediction

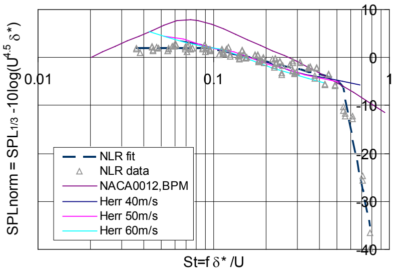

Problem area

Acoustic and aerodynamic measurements were carried out on a flat plate in NLR's Small Anechoic Wind Tunnel KAT. The test campaign was part of the European project Advanced Flow Diagnostics for Aeronautical Research (AFDAR). The main objective of the experiments was to provide a benchmark for noise predictions based on time-resolved Tomographic PIV flow measurements.

Description of work

The trailing edge noise and flow properties of a flat plate for different wind speeds and trip methods were determined. In order to isolate the trailing edge noise from extraneous noise sources, acoustic measurements were done using a 48-microphone phased array. Hotwire measurements were performed just behind the wedged trailing edge of the plate to determine the boundary layer shape and turbulence intensity. The quality of the data has been assessed and several scaling laws were investigated.

Results and conclusions

A database containing acoustic and aerodynamic measurements for a flat plate configuration has been obtained. Tripped (carborundum and zigzag tape) and clean configurations have been considered at varying wind speeds (15m/s to 75m/s). The broadband trailing edge data gave the best collapse when it was scaled with $U^{4.5}$. In general it can be concluded that the experimental data is of good quality.

Applicability

A benchmark has been obtained that can be used to evaluate PIV based noise prediction algorithms.

Report no.
NLR-TP-2012-332

Author(s)
M. Tuinstra
S. Oerlemans
J.H.M. Gooden

Report classification
UNCLASSIFIED

Date
August 2013

Knowledge area(s)
Aëro-akoestisch en experimenteel aërodynamisch onderzoek

Descriptor(s)
Trailing edge noise
flat plate
PIV
Noise prediction
AFDAR

This report is based on a presentation held at the International workshop on the application of particle image velocimetry for aeroacoustics and noise, Delft, Netherlands, 16-04-2012.

Nationaal Lucht- en Ruimtevaartlaboratorium, National Aerospace Laboratory NLR

Anthony Fokkerweg 2, 1059 CM Amsterdam,
P.O. Box 90502, 1006 BM Amsterdam, The Netherlands
Telephone +31 88 511 31 13, Fax +31 88 511 32 10, Web site: www.nlr.nl

NLR-TP-2012-332

Trailing edge noise: A benchmark for PIV based noise prediction

M. Tuinstra, S. Oerlemans and J.H.M. Gooden

This report is based on a presentation held at the International workshop on the application of particle image velocimetry for aeroacoustics and noise, Delft, Netherlands, 16-04-2012.

Customer	European Commission
Contract number	AFDAR
Owner	NLR
Division NLR	Aerospace Vehicles
Distribution	Unlimited
Classification of title	Unclassified
	August 2013

Approved by:

Author	Reviewer	Managing department
M. Tuinstra	J.H.M. Gooden	J. Hakkaart
Date: 29/08/13	Date: 30/8/13	Date: 30/8/13

Contents

This page is intentionally left blank.

Trailing edge noise: A benchmark for PIV based noise prediction

M. Tuinstra, S. Oerlemans and J.H.M. Gooden
National Aerospace Laboratory NLR, Emmeloord, The Netherlands

Acoustic and aerodynamic measurements were carried out on a flat plate in NLR's Small Anechoic Wind Tunnel KAT. The test campaign was part of the European project Advanced Flow Diagnostics for Aeronautical Research (AFDAR). The main objective of the experiments was to provide a benchmark for noise predictions based on time-resolved Tomographic PIV flow measurements. The trailing edge noise and boundary layer of a flat plate with a wedged trailing edge for different wind speeds and trip methods were determined. In order to isolate the trailing edge noise from extraneous noise sources, acoustic measurements were done using a 48-microphone phased array. Hotwire measurements were performed just behind the trailing edge of the plate to determine the boundary layer shape and turbulence intensity. The quality of the data has been assessed and several scaling laws were investigated. The broadband trailing edge data gave the best collapse when it was scaled with $U^{4.5}$. In general it can be concluded that the experimental data is of good quality.

A. Introduction

In the European project Advanced Flow Diagnostics for Aeronautical Research (AFDAR) state-of-the-art Particle Image Velocimetry (PIV) techniques are evaluated and developed. One AFDAR objective is to demonstrate the feasibility of noise prediction based on PIV data. Lorenzoni et al.[1,2] showed for a rod-airfoil configuration that time-resolved (TR) planar PIV measurements allow the calculation of the hydrodynamic pressure field and the related acoustic emission. The tonal noise component, resulting from the impingement of a quasi-2D vortex roller, shed from the rod onto the airfoil, could be adequately predicted by application of Curle's analogy[3]. The broadband noise prediction showed less agreement with noise measurements as a result of the three dimensional nature of the noise generating flow structures. Continuing this work, the feasibility of broadband noise prediction based on measured flow field data will be evaluated in AFDAR.

Broadband trailing edge (TE) noise emission of a flat plate configuration is to be investigated. Based on theory[4] it has been suggested that the interaction of the two boundary layers at the TE could be of relevance to TE noise. Experiments by Brooks et al.[5], however, showed no evidence supporting this hypothesis. Furthermore, they showed that TE noise could be predicted based on surface pressure measurements acquired on a single side of the trailing edge. To make a flow-based acoustic prediction it is therefore sufficient to measure the boundary layer on a single side of the trailing edge with a measurement volume large enough to capture the largest coherent flow structures. To relate turbulent eddies washing over the trailing edge with their acoustic emission into the far field, an analytical formulation of the Green's function for a semi-infinite plate is available[6]. Note that a more complex geometry would quickly require a numerical assessment of the Green's function, e.g. by Boundary

Element Methods. The above makes the flat plate configuration particularly suitable to investigate PIV based noise predictions.

In this paper acoustic measurements will be presented for a flat plate configuration of finite thickness, provided with a wedged trailing edge. These results will serve as benchmark for PIV-based noise predictions. The test was conducted in NLR’s Small Anechoic Wind Tunnel (KAT). A 48-microphone phased array was used to conduct acoustic measurements. The near-TE wake flow (5mm behind the TE) was measured by hotwire. The measurements were done for a range of flow speeds (15m/s to 75m/s, Reynolds number based on chord length Re =6.0 10^5 to 3.0 10^6), both for a tripped and clean plate. All measurements were taken at an angle of attack of zero degrees.

The paper is outlined as follows: Section B will treat the experimental setup. This is followed by Section C in which the phased array processing procedures used to obtain trailing edge noise spectra are explained. Then in Section D and E respectively, the flow and acoustic measurement result are presented. The conclusions of the work are provided in Section F.

B. Test setup

The tests were carried out in NLR's Small Anechoic Wind Tunnel. The KAT is an open circuit, open jet wind tunnel. The test section is surrounded by a 5x5x3 m^3 room which is completely covered with 0.5 m foam wedges, yielding more than 99% absorption above 500 Hz. Two horizontal endplates (0.90x0.70 m^2) are mounted to the upper and lower sides of the rectangular 0.38x0.51 m^2 nozzle, providing a semi-open test section for airfoil self-noise measurements (see Figure 1 and Figure 2). To suppress reflections, the endplates are acoustically lined with a 5.5 cm layer of sound absorbing foam covered by a 5% open perforated plate.

The aluminium flat plate (Figure 3) has a chord length of 599 mm and a span of 509 mm. It has an elliptical leading edge shape and a wedged trailing edge, connected by a flat surface. The thickness of the plate equals 10 mm and at the TE has a wedge angle of approximately 5 degrees. The plate was mounted vertically between the endplates at zero angle of attack. The thickness at the TE is less than 200μm. The flat plate was tested for clean and tripped conditions.

The boundary layer on the plate was tripped (Figure 4) with carborundum 24 (nominal grain size 0.84 mm) or Streifeneder zigzag tape (0.7 mm thickness) over the complete span. A carborundum trip generally yields homogeneous turbulence characteristics along the span. Whereas, in case of a zigzag trip, traces of spanwise turbulence variation can remain. Nevertheless, it was added in order to obtain a well-reproducible trip method. The thickness of 0.7 mm was chosen on the basis of XFOIL calculations, carried out to determine a roughness corresponding that of the carborundum trip. The trips were applied on both sides of the plate and started 100 mm downstream of the leading edge along the chord line. The carborundum trip had a streamwise width of 10 mm; the streamwise peak-to-peak distance of the zigzag trip was 11 mm. The 0.7 mm zigzag trip was obtained by applying 0.3-mm and 0.4-mm trips on top of each other. The carborundum grains were applied using an adhesive spray. The functioning of the trips was verified at the lowest wind speed of 15 m/s using a stethoscope.

Hotwire measurements were carried out with a DANTEC StreamLine CTA system. The hotwire probe was mounted on a traversing system with an elliptical support strut that allows positioning with an accuracy of 0.1mm. A single wire probe (DANTEC 55P01) was used with the wire oriented vertically, parallel to the flat plate trailing edge. The wire sensor length amounts to 1.25 mm and the wire diameter to 5 μm.

The microphone array consisted of 48 ½-inch microphones (type LinearX M51) mounted in an open grid and was designed for maximum side-lobe suppression at frequencies between 1 and 20 kHz. All microphones, except for two closely spaced microphones at the centre of the array, were equipped with wind screens. To obtain high resolution at low frequencies, the array dimensions needed to be rather large (0.8 x 0.6 m^2). The array was placed outside the tunnel flow at a distance of 0.6 m from the tunnel axis, on the starboard side of the model. The relatively small distance between the array and the model was chosen to obtain maximum signal-to-noise ratio and resolution. The centre of the array was placed at the same height as the tunnel axis

C. Array processing

The acoustic data from the array microphones were synchronously measured using the VIPER data-acquisition system[7]. The data were acquired with a sample frequency of 30720 Hz for a measurement time of 30 s. A 500Hz high-pass filter and 15360 Hz low-pass filter were applied to the signal before the AD converter. Before and after the measurements, the sensitivity at 1 kHz was checked for all array microphones using a calibrated pistonphone. Frequency-dependent sensitivities of individual microphones were taken from calibration sheets. No corrections were applied for microphone directivity, because this effect is the same for the different configurations and amounts to less than 2 dB for angles up to 45° and frequencies up to 15 kHz. Phase matching of the microphones was checked prior to the measurements using a calibration source at a known position.

The array data were processed using the SOLACAN software[8], which produces acoustic source maps in 1/3-octave bands using conventional beamforming. In this way, noise originating from the model is separated from background noise. To improve the resolution and further suppress background noise from the tunnel, the main diagonal in the cross-power matrix (auto-powers) was discarded. The effect of sound refraction by the tunnel shear layer was corrected using a simplified Amiet method[9], where the shear layer centre was assumed to be at the same y location as the edge of the tunnel nozzle. Furthermore, a spatial window was applied to the microphone signals, in order to correct for the variation in microphone density over the surface of the array. Finally, another spatial window was applied which reduces the effective array aperture with increasing frequency, in order to reduce coherence loss effects. The array scan plane was placed in the surface plane of the flat plate. The density of the scan grid was 1 cm in both the streamwise and vertical direction, and the scan levels were normalized to a distance of 0.282 m $[(4\pi)^{-1/2}]$, so that for a monopole source the peak level in the source plot corresponds to the Sound Power Level.

To illustrate the expected resolution of the array, Figure 5 shows simulated source maps for an uncorrelated line source at the trailing edge for the present set-up. It can be seen that the resolution increases with frequency, due to the decreasing acoustic wavelength.

For quantitative comparison of different conditions, the array results were further processed using a power integration method, which produces narrowband and 1/3-octave band spectra for specific source regions. Again the main diagonal in the cross-power matrix was discarded, and spatial windows were applied to the microphone signals to reduce coherence loss effects. Thus, the levels measured by the array represent noise levels radiated in the average direction of the array microphones, including the weighting as a result of the spatial windows. Because the source directivity for trailing edge noise is expected to be the same for all conditions, the comparison of sound levels from different conditions is valid.

The procedure as in [10] was followed to determine trailing edge noise spectra from the integrated spectra. By defining an integration contour around the mid-span area of the model, background noise and possible extraneous noise sources at the model-endplate junctions were suppressed. The mid-span integration area was centred on the trailing edge. The size of the integration area was 0.2 m in chordwise direction and 0.1 m in spanwise direction, and the scan resolution was 1 cm in both the streamwise and vertical direction. Since the integration area 'cuts' through the line source region at the trailing edge, 'leakage' from source regions outside the integration area into the integration contour, and vice versa, will occur. The magnitude of this effect depends on array resolution, and therefore on frequency. To account for this effect, a line source correction was applied to the integrated levels, which was determined from simulations. The resulting spectral levels are Sound Power Levels produced by 10 cm of span.

Despite the use of the trailing edge integration contour, for some conditions (trip configuration, wind speed, frequency), the trailing edge noise levels were influenced by background noise from the wind tunnel. The tunnel background noise was quantified by performing acoustic measurements without model for all wind speeds. In order to allow fast judgment of the validity of the measured levels, background noise was accounted for as follows. If the signal-to-noise ratio (i.e. the difference between the measurement with plate and without plate) is larger than 3 dB (10log2), the trailing edge noise level is corrected for background noise on a pressure-squared basis, and the level is assumed to be valid. If the signal-to-noise ratio is smaller than 3 dB, no correction is applied and the level represents an upper limit for the actual trailing edge noise level. A valid trailing edge noise level is indicated by a marker in the spectrum.

D. Flow characteristics

D.1 Average velocity and turbulence intensity distribution

Velocity and turbulence intensity distributions were measured at 5mm behind the trailing edge. Figure 6, Figure 7 and Figure 8 show the results for the clean configuration, carborundum trip and zigzag trip respectively. In this G represents the magnitude of the local velocity vector and G_r the freestream velocity. The velocity distribution for the clean configuration shows velocities of nearly zero in the centre at the lowest reference speed of 15m/s. Furthermore the turbulence intensity shows high values (even exceeding 2 when normalized with local average velocity, not shown here). A hotwire is not able to measure reverse flow and hence the measured velocity is inaccurate for this condition. However this is a strong indication that flow separation occurred. At 45 and 75 m/s the flow possesses turbulent characteristics.

For the tripped configurations the following is noted. Except for 15 m/s the minimum flow velocity in the centre of the wake is almost equal ($G/G_r \approx 0.45$) for both trips. Both the velocity and turbulence intensity distribution show a similar trend and magnitudes are of the same order. For the zigzag trip slightly more Reynolds number dependency is found. Both configurations show a stronger

Reynolds number dependency on the Y<0 side. The reason for this possibly lies in the quality of the surface, in particular the finishing of the leading edge that is different for both sides. This may cause small flow convergence/divergence effects that quickly affect the local boundary layer thickness. Also the different model parts just in front of the trailing wedge have more or less different accurate fittings on both sides of the model. Negative Y-values correspond to the side of the model that was on the side of the acoustic array.

D.2 Displacement thickness

Displacement thickness is a flow parameter commonly used to scale noise levels associated with TE noise and to normalize the frequency in terms of a Strouhal number. The displacement thickness has therefore been calculated from measurements. The displacement thickness of one side of the wake is defined as:

$$\delta^* = \int_{Yp_{U_{\min}}}^{Yp_{U=U_e}} \frac{\rho_{inv} G_{inv} - \rho\, G}{\rho_{inv_e} G_{inv_e}}\, dYp \qquad (1)$$

where G is the actual (measured) velocity, G_{inv} represents an assumed inviscid velocity, and the subscripts $_{\min}$ and $_e$ indicate the minimum and edge of the wake (to be defined below). Often G_{inv} is simply taken to be equal to freestream velocity. However, this is less accurate since inviscid velocity deficits related to static pressure changes do not contribute to the displacement thickness. The inviscid velocity is determined solely by the local static pressure (zero total pressure loss, so no viscous wake, is assumed). As the static pressure is not measured in this test, the inviscid velocity distribution is determined by a 4th order polynomial fit between the velocity measurements outside of the wake. The 'inviscid' region has been identified by using the local turbulence intensity g' as a discriminator. Datapoints located in a window between the minimum value of g' at both ends of the distribution and this minimum plus 0.02 times the difference between maximum and minimum value of g' are termed as 'inviscid'. The partition between both wake halves has been taken as coinciding with the minimum wake velocity. The displacement thicknesses for both sides of the wake have been determined using a trapezoidal integration over the relevant wake side. The complete wake displacement thickness is the sum of the displacement thicknesses of both wake halves. Furthermore displacement thickness of the wake has also been determined from a boundary layer calculation by means of XFOIL, both for natural transition and with a trip at 10% chord.

XFOIL calculations show that for the tripped case a nearly standard $Re^{-0.2}$ behaviour is obtained (Figure 9). The actual measurements however, show a smaller exponent, around -0.12. This is likely the result of overtripping of the boundary layer, in particular at the higher Reynolds number. Consequently, an additional thickening of the boundary layer and therefore a δ^*-penalty occurs. The overtripping tendency seems to be less for the zigzag trip than for the carborundum trip.

The predicted behaviour for natural transition also differs from the actual measurement. Note that the lowest velocity has been omitted here, due to the presence of flow separation, which was not predicted by XFOIL. For the two highest Reynolds numbers no flow separation is observed. Nevertheless, the XFOIL calculation shows significantly lower δ^*-values than measured. A marked difference between XFOIL and the actual test is that the actual test shows a fairly long transition trajectory with gradually increasing turbulent intermittency, whereas XFOIL assumes transition to occur suddenly. It is hypothesized that the intermittently laminar boundary layer exhibits a stronger growth rate than a fully turbulent boundary layer (as predicted by XFOIL) since the less energetic laminar flow has more difficulty to remain attached at the transition from the flat surface to the wedge-shaped trailing edge.

The δ^* for each wake half (separated at the minimum velocity point) has been calculated since the previous section indicated a slight asymmetry of the wake. Figure 10 confirms that indeed the wake half on the array side ('as') grows slightly stronger (~10% difference) than on the opposite side ('os'), resulting in a greater displacement thickness. This can be explained by convergent/divergent flow as mentioned earlier. Another explanation could be a small wind tunnel flow angularity or model misalignment.

Therefore additional XFOIL calculations have been performed with a small angle of attack of 0.5^o. The results are also shown in Figure 10. The XFOIL results show a constant offset in δ^* and not the divergence between both curves as found in the measured curves. Therefore it seems unlikely that wind tunnel flow angularity/model misalignment is the cause of the divergent curves. The most plausible reason is still a slight non two-dimensionality of the flat plate model.

D.3 Spectra

The turbulence spectra are plotted for the carborundum (Figure 11) and zigzag (Figure 12) configuration at y=2mm, corresponding to a region of high turbulence intensity. When the spectra are compared they qualitatively and quantitatively show the same image.

Until $k \approx 300$, a k^{-1} decay of the energy is found, followed by a steeper $k^{-5/3}$ decay that also follows from Kolmogorov's [11,12,13] theory for isotropic turbulence. In terms of flow structures, the part of the spectrum that follows k^{-1} can be interpreted as a region of turbulence production and is associated with large scale flow structures. The inertial range ($k^{-5/3}$) is related with the breakup of large scale flow structures in to smaller flow structures, which in turn breakup themselves to provide an energy cascade from low wave numbers to high wave numbers. This region of the flow is dominated by inertial forces. After an intermediate range, where both viscous and inertial forces play a role the viscous range follows which according to theory should obey a k^{-7} decay. This range is however not apparent in the spectra as the measured frequency does not extend to that range.

E. Noise spectra

E.1 Source maps

The acoustic source maps for the flat plate with carborundum trip at different wind speeds are shown in Figure 13 to Figure 16. The dB scale is adjusted for each map however the range is always 12 dB. The black line indicates the position of the trailing edge and flow is from left to right. Similar to the simulations (Figure 5), the resolution increases with increasing frequency. The appearance of the line sources in Figure 14 is very similar to the simulations. For increasing wind speed the line sources appear at higher frequencies, which is typical for trailing edge noise (more clearly seen in Figure 20). At high wind speeds, tunnel noise is dominant for the low frequencies. The reason for the increased levels above and below the tunnel axis at 20 m/s between 1.6 kHz and 2.5 kHz (Figure 13) is not known. This phenomenon was repeatable and was also visible at 15 m/s. The source maps for the other plate configurations showed similar output. The most important conclusion is that we indeed measure trailing edge noise and not extraneous noise sources.

E.2 Repeatability of trailing edge noise spectra

The trailing edge noise spectrum was determined from the source maps by applying the power integration method to the mid-span part of the trailing edge. The repeatability of the trailing edge noise spectra is illustrated in Figure 17 (left) for the carborundum trip. As was explained earlier, a marker indicates a valid sound level, while the absence of a marker indicates that the value shown is an upper limit for the actual trailing edge noise level. The range of the dB scale in the trailing edge noise spectra is always 50 dB. Despite differences in Reynolds number of a few percents (due to temperature differences), the levels generally reproduce within a few tenths of a dB. For the clean plate (Figure 17, right) larger differences are found at the lowest speeds, presumably due to the sensitivity of the boundary layer transition to the surface conditions.

E.3 Effect of tripping

Figure 18 compares the trailing edge noise spectra for the clean plate and the carborundum plate at all measured wind speeds. At low wind speeds large differences occur, due to the fact that the clean plate has a transition trajectory while the tripped plate exhibited transition directly behind the trip. At the lowest speed of 15 m/s the clean plate is quieter than the tripped plate due to the thinner boundary layer, while at 45 m/s and 75 m/s the spectra practically coincide because the boundary layers are almost identical (see Section E for details). For 20 m/s and 25 m/s the clean plate is noisier than the tripped plate.

The trailing edge noise spectra for the different trip are compared in Figure 19. Despite small differences, the results for the carborundum trip and the zigzag tape are very similar, in line with the hotwire results.

E.4 Effect of wind speed

The effect of wind speed on the trailing edge noise is shown in Figure 20 for the carborundum trip and zigzag tape. As expected, both the levels and the dominant frequencies increase with increasing wind speed. According to aeroacoustics theory[14], the sound levels are expected to scale according to $p^2 \sim U_t^5$, with p the acoustic pressure and U_t the tunnel speed. The dominant frequencies are expected to be proportional to U_t. The result of applying this scaling (normalized sound levels versus Strouhal number) is shown in Figure 21. It can be seen that the spectra for the different wind speeds collapse within about 5 dB.

A better data collapse may be obtained by using the boundary layer displacement thickness at the trailing edge length to scale the levels and frequencies[14]. On the basis of the hotwire results, the displacement thickness was found to scale with Reynolds number as follows: $\delta^*_{exp} \approx 0.04 \cdot C \cdot \mathrm{Re}^{-0.12}$. The result is shown in Figure 22. It appears that the data collapse hardly improves with respect to the previous figure. Estimating the displacement thickness using the theoretical relation[15] $\delta^* \approx 0.05 \cdot C \cdot \mathrm{Re}^{-0.2}$ did not improve the data collapse either (not shown). The best data collapse is obtained by scaling the levels using a speed exponent of 4.5 instead of the theoretical value of 5

(Figure 23). Previous studies on trailing edge noise[10] and slat noise[16,17], which may be regarded as a TE noise mechanism, also showed that scaling with an exponent of 4.5 yields the best data collapse. This slightly reduced exponent may be physical or may be due to coherence loss, which may slightly reduce the integrated spectral levels at high speeds and frequencies, despite the use of an integration contour.

E.5 Comparison to single and array averaged microphone levels

The power integration method is validated by comparison to single microphone and array averaged noise levels. TE noise for the clean configuration at U_t=25m/s was found louder (see E.3) than that of the tripped configurations and sufficiently superseding background noise to be able to carry out above comparison. All noise levels were corrected for wind tunnel background noise. Furthermore, to compare results directly the sound power levels were expressed in sound pressure levels at the microphone location:

$$SPL_{norm} = PWL_{norm} - 10\log 4\pi r^2 + 10\log\frac{s}{s_0} \tag{2}$$

In this r is the distance from the TE to the microphone, s the span of the plate and s_0 the span that the power level (PWL) represents. For this case r=0.6 m, s=0.5 m and s_0=0.1 m. Results are shown for those frequencies where TE noise superseded background noise by at least 3dB.

Figure 24 shows the spectrum at a distance r=0.6m from the TE as was measured by the phased array centre microphone (red line) and the average spectrum over all microphones (cyan line). The diamond markers indicate the spectrum that was obtained from the power integration approach. Good agreement is found with the single microphone measurement. Differences are in the order of 1dB. Excellent agreement is found with the array averaged spectrum, with differences in the order of 0.5dB. It is noted that at the lowest and highest frequencies the single microphone and array averaged measurements appear to be contaminated by background noise, providing higher noise levels than the power integration method. This is not surprising, considering that at the threshold of 3dB above background noise levels, background noise and TE noise are of equal strength.

E.6 Comparison to existing noise measurements

Although there is an abundance of work reported on airfoil trailing edge noise, studies dealing with flat plate trailing edge noise are less common. A significant body of work is that of Herr[18,19,20], who used flat plate configurations to study trailing edge noise and means to reduce it. TE noise spectra for a 0.8m flat plat at U_t=40m/s, 50m/s and 60m/s were taken from [19], Figure 4a. The spectra were rescaled using $U^{4.5}$ and δ^* and compared with the NLR data acquired for the carborundum trip (Figure 25). The current data was expressed in SPL by (2) to match the Herr experiment (r=1.15m, s=0.8m). A generic spectrum shape for flat plate trailing edge noise is obtained by a regression fit and also plotted in Figure 25. The data is split in three regions, for which we obtain:

$$PWL_{norm} = SPL_{norm} + 10\log 4\pi r^2 - 10\log\frac{s}{s_0} = \begin{cases} 0.11\ \mathrm{logSt} + 5.2 & \text{for} \quad \mathrm{St}<0.1 \\ -9.1\mathrm{logSt} - 4.0 & \text{for } 0.1<\mathrm{St}<0.53 \\ -188.9\ \mathrm{logSt} - 52.9 & \text{for} \quad \mathrm{St}>0.53 \end{cases} \tag{3}$$

Firstly it is noted that also for the Herr experiment a better collapse of the spectra is obtained when normalizing with $U^{4.5}$. Comparing the two datasets, good agreement is found for St>0.1 showing the same decay with Strouhal number. For St<0.1 the present data shows an approximately constant level whereas Herr reports a continuous increase. In the same figure a predicted[14] noise spectrum for a NACA0012 airfoil at 40m/s is plotted (as shown in [19]), which does not collapse with the flat plate TE spectra. Since the geometry is not that different, the explanation must be sought in the boundary layer flow characteristics. The spectrum obtained from the current data flattens out in the same Strouhal range at which the NACA0012 spectrum attains its maximum. It is difficult though to identify where the maximum occurs exactly.

F. Conclusions

Acoustic and aerodynamic measurements on a flat plate have been carried out in NLR's Small Anechoic Wind Tunnel KAT. The main objective of the experiments was to provide a benchmark for PIV-based noise predictions.

A database containing acoustic and aerodynamic measurements for a flat plate configuration has been obtained. Tripped (carborundum and zigzag tape) and clean configurations have been considered at a number of wind speeds (15m/s to 75m/s).

For the clean configuration, a transition trajectory occurs along the plate, penalizing reproducibility. Hotwire measurements show minimal differences between the carborundum and zigzag trip configurations. The Reynolds dependency of boundary layer thickness for the tripped configurations was lower than predicted by theory ($Re^{-0.2}$). This was attributed to overtripping of the boundary layer at higher Re. A slight asymmetry was found in the wake profiles, attributed to small non two-dimensionalities in the leading edge of the flat plate. Turbulence spectra show a region of turbulence production and an inertial range that follows the $k^{-5/3}$ law as is predicted by theory for isotropic turbulence.

The power integration method was validated by comparison to single microphone and array averaged levels. Comparison with TE noise spectra found in literature showed good agreement for S_t>0.1. For the present data set, a $U^{4.5}$ scaling gave the best spectrum collapse. This could be caused by coherence loss at flow velocities, which would result in a lower measured acoustic level. On the other hand, $U^{4.5}$ scaling has been reported to provide good data collapse for several independent experiments now, which might indicate that it is a real phenomenon. Acoustic measurements for the tripped configurations were reproducible within a few tenths of a dB. The clean configuration showed a larger scatter on repeat measurements. Comparisons of the acoustic emission for both trips showed only small differences. In general it can be concluded that the experimental data is of good quality.

References

1. V. Lorenzoni, M. Tuinstra, P. Moore and F. Scarano, *"Aeroacoustic analysis of a rod-airfoil flow by means of time-resolved PIV"*, AIAA-2009-3298, 2009
2. V. Lorenzoni, F. Scarano and M. Tuinstra, *"On the Use of Time-Resolved Particle Image Velocimetry for the Investigation of Rod-Airfoil Aeroacoustics",* to be published
3. N. Curle, *"The influence of solid boundaries upon aerodynamic sound"*, Proc. Roy. Soc. Lon., Vol. A 211, 1952, pp.564-587
4. M.S. Howe, *"A review of theory of trailing edge noise*", Journal of sound and vibration, 61, 437-465, 1978
5. T.F. Brooks and T.H. Hodgson, "*Trailing edge noise prediction from measured surface pressures"*, Journal of sound and vibration, 78(1), 69-117, 1981
6. J.E. Ffowcs Williams and L.H. Hall, *"Aerodynamic sound generation by turbulent flow in the vicinity of a scattering half plane"*, Journal of fluid mechanics, vol.40, no.4, 1970, pp657-670
7. H. Holthusen and H. Smit, "*A new data-acquisition system for microphone array measurements in wind tunnels"*, AIAA paper 2001-2169, 2001
8. P. Sijtsma, "*Users guides of acoustic array data processing software - Extended issue; version 7.0"*, NLR-TR-2009-528, 2009
9. R.K. Amiet, "*Refraction of sound by a shear layer"*, Journal of Sound and Vibration, Vol. 58, No. 2, pp 467-482, 1978
10. S. Oerlemans, *"Wind Tunnel Aeroacoustic Tests of Six Airfoils for Use on Small Wind Turbines"*, NREL/SR-500-35339, May 2004.
11. A.N. Kolmogorov, *"The local structures of turbulence in incompressible viscous fluids vor very large Reynolds numbers"*, Comp.rend., Acad. Sci. URSS, vol.30, no.4, 1941
12. A.N. Kolmogorov, *"Dissipation of energy in Locally Isotropic turbulence"*, Comp.rend., Acad. Sci. URSS, vol.32, no.1, 1941
13. W. Heisenberg, *"Zur statistischen theorie der turbulenz "*, Zeitschr. Phys., Bd.124, Heft 7/12, 1948
14. T.F. Brooks, D.S. Pope and M.A. Marcolini, "*Airfoil self-noise and prediction"*, NASA Reference Publication 1218, 1989.
15. H. Schlichting, *"Boundary-Layer theory*", McGraw-Hill, 1979.
16. M. Pott-Pollenske, W. Dobrzynski, H. Buchholz, B. Gehlar and F. Walle, *"Validation of a semiemperical airframe noise prediction method through dedicated A319 flyover noise measurements"*, AIAA 2002-2470, 2002
17. M. Pott-Pollenske, J. Alvarez-Gonzales and W. Dobrzynski, *"Effect of slat gap on farfield radiated noise and correlation with local flow characteristics"*, AIAA 2003-3228, 2003
18. M.Herr and W. Dobrzynski, *"Experimental Investigations in low noise trailing edge design"*, AIAA 2004-2804, 2004
19. M.Herr, *"A noise reduction study on flow-permeable trailing-edges"*, DLR electronic library, 2007
20. M.Herr, *"Trailing-edge noise data quality assessment for CAA validation"*, AIAA 2010-3877

Figures

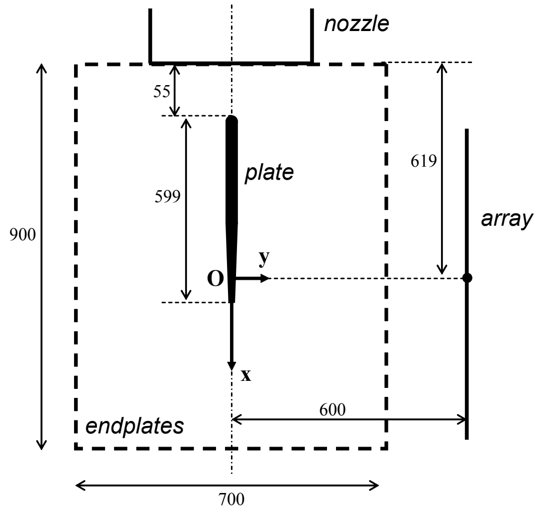

Figure 1 - Top view of KAT set-up for trailing edge noise measurements. The microphone array was located on the +y side of the model. The origin of the coordinate system is on the tunnel axis, aligned with the array center. Dimensions in mm (not to scale)

Figure 2 - KAT set-up with microphone array and flat plate vertically mounted between the lined endplates

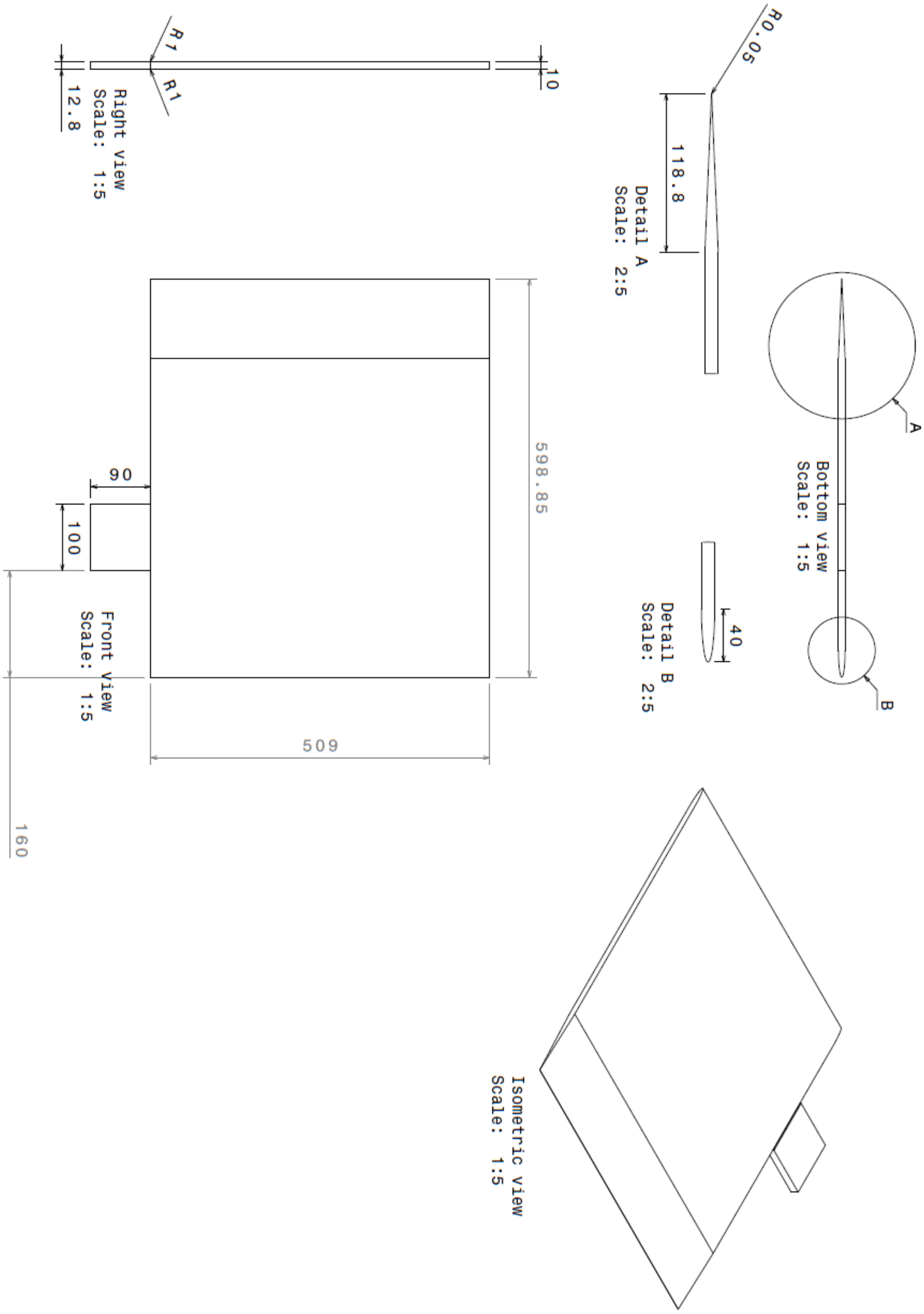

Figure 3 - Design details of the flat plate

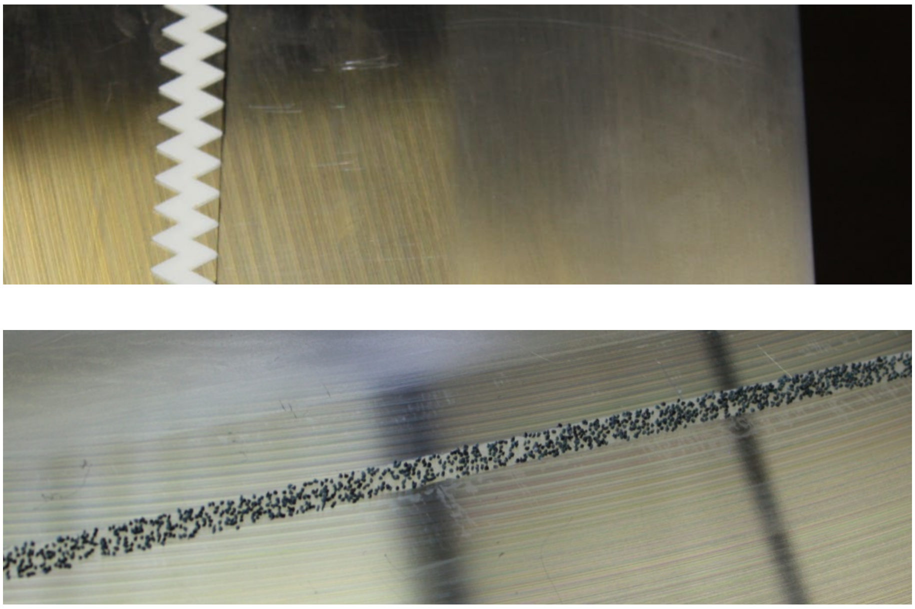

Figure 4 - Above: Zigzag trip; Below: Carborundum trip

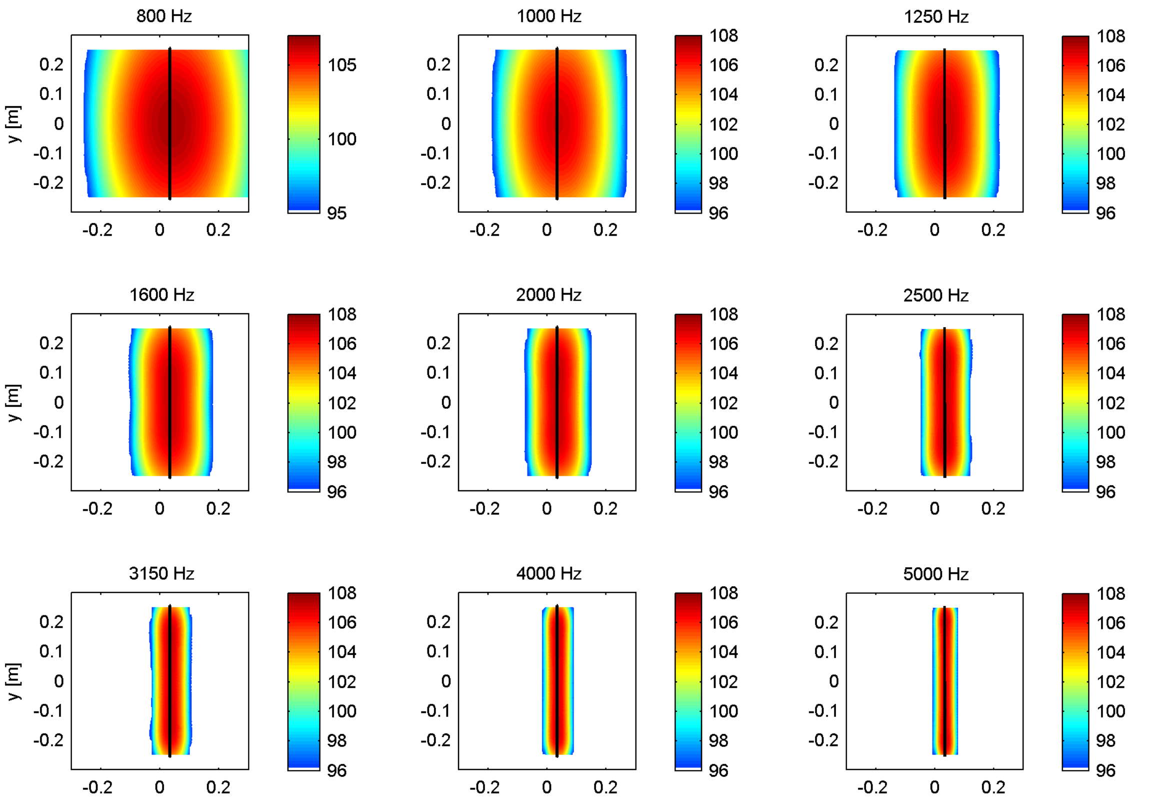

Figure 5 - Simulated source maps for an uncorrelated line source (white noise) at the trailing edge. Flow is from left to right and the range of the colour scale is 12 dB. The black line indicates the position of the trailing edge

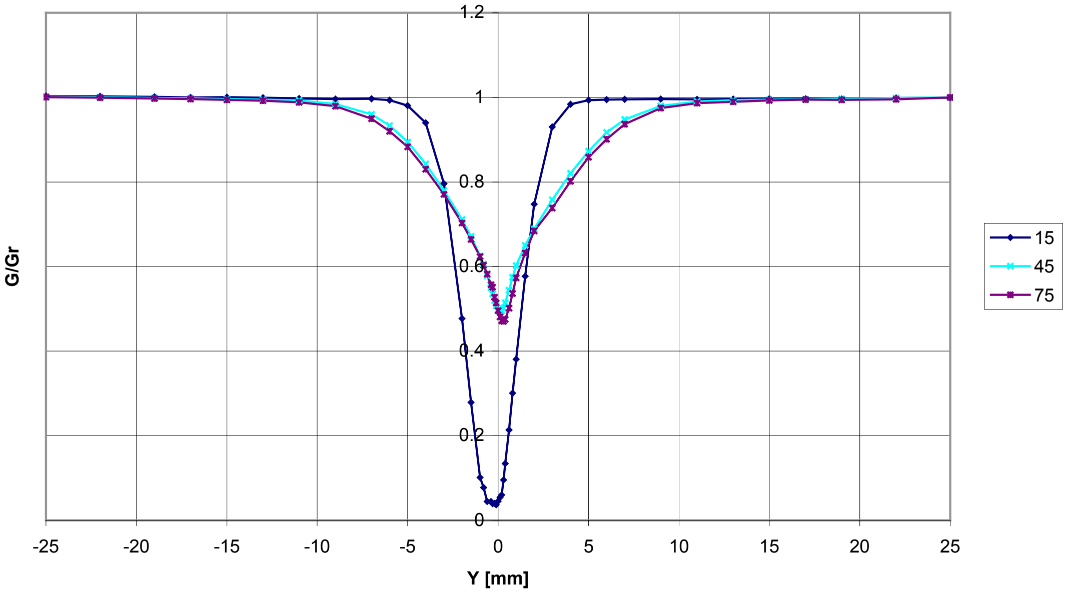

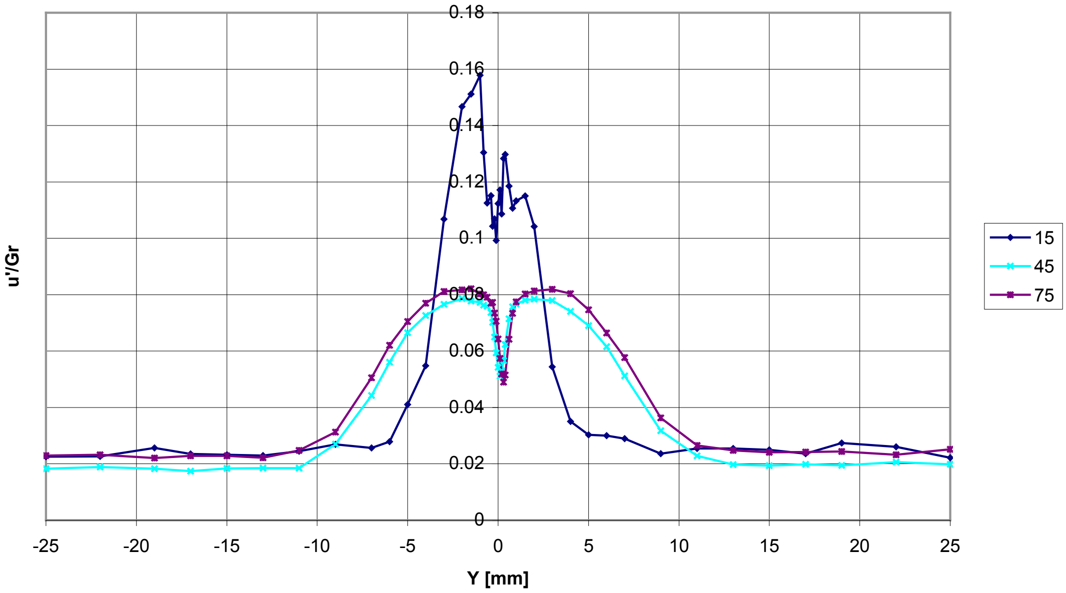

Figure 6 - Clean configuration, G_r=15m/s, 45m/s and 75m/s; Above: Normalized local mean velocity; Below: Turbulence intensity normalized with reference mean velocity

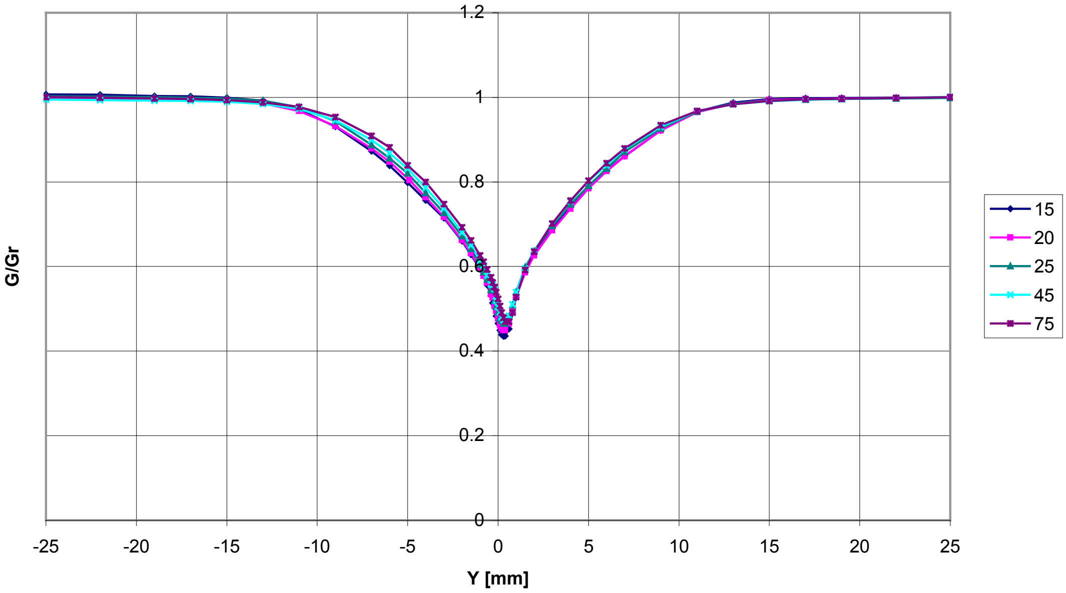

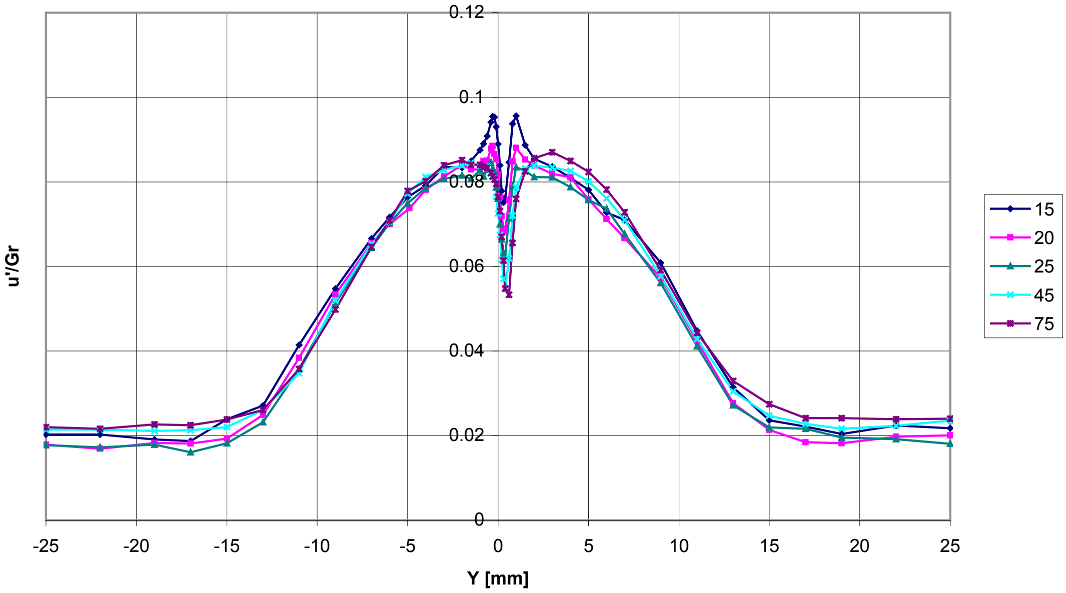

Figure 7 - Carborundum configuration, G_r=15m/s, 20m/s, 25m/s, 45m/s and 75m/s; Above: Normalized local mean velocity; Below: Turbulence intensity normalized with reference mean velocity

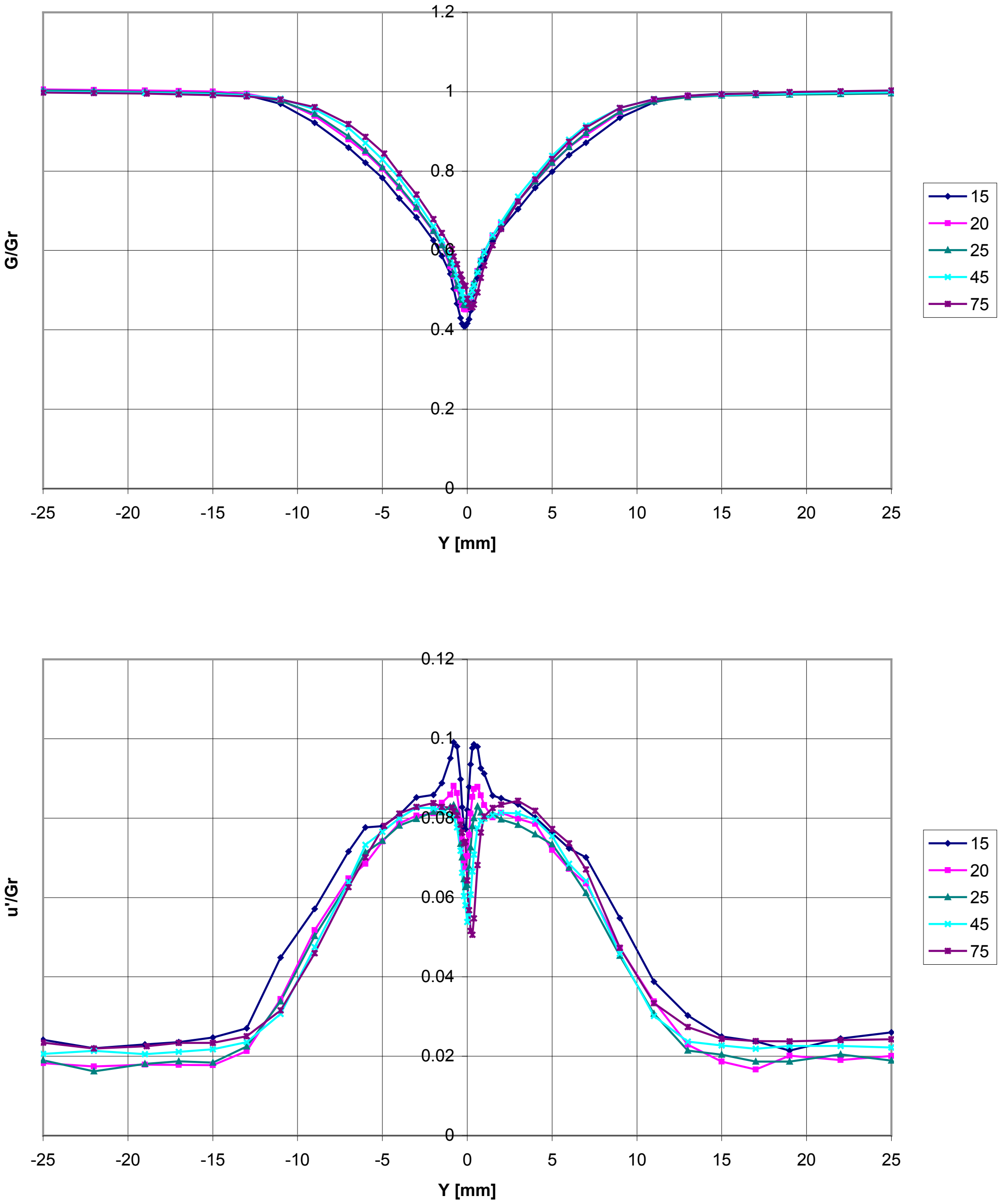

Figure 8 - Zigzag configuration, G_r=15m/s, 20m/s, 25m/s, 45m/s and 75m/s, Above: Normalized local mean velocity; Below: Turbulence intensity normalized with reference mean velocity

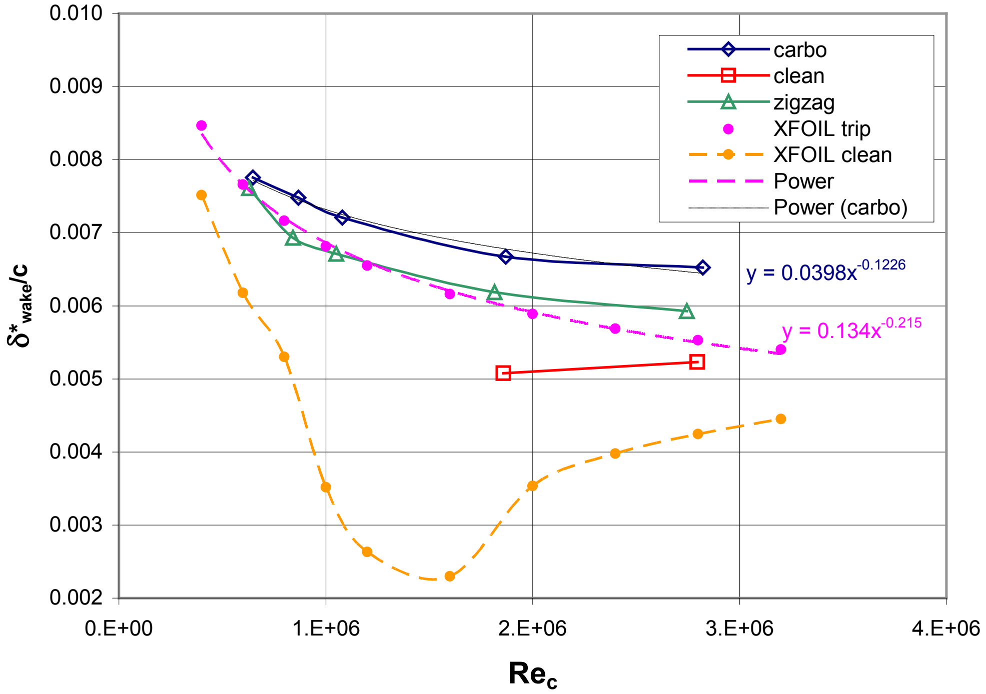

Figure 9 - Calculated and measured displacement thickness at trailing edge

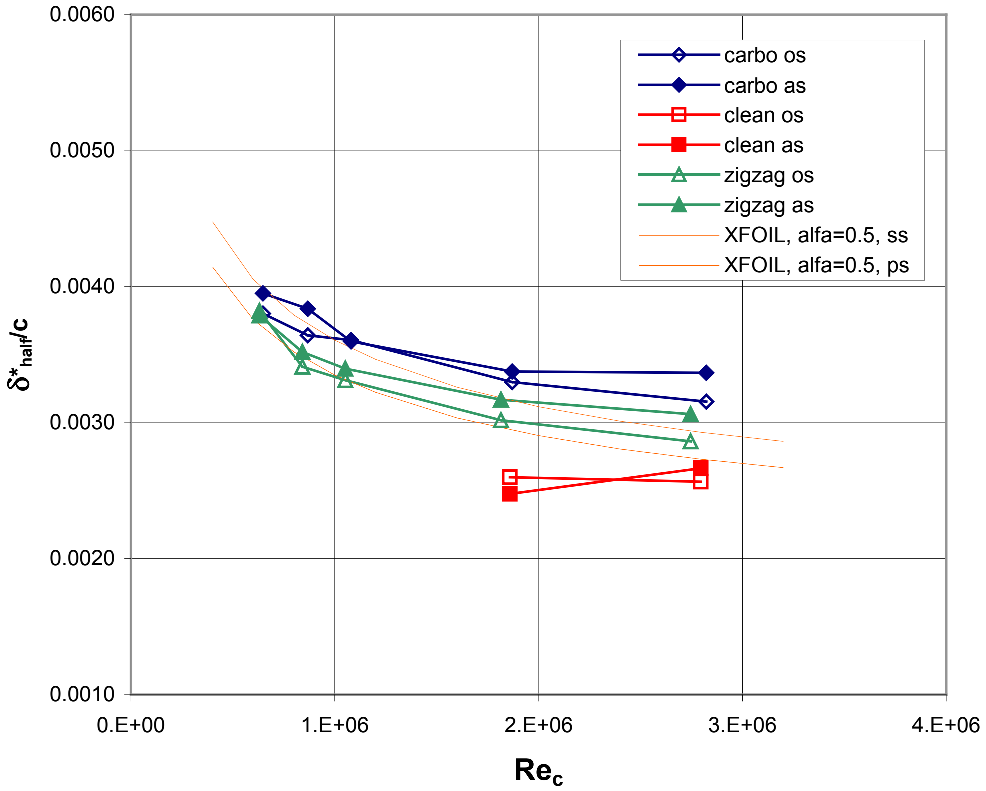

Figure 10 - Calculated and measured displacement thickness on both sides of the trailing edge

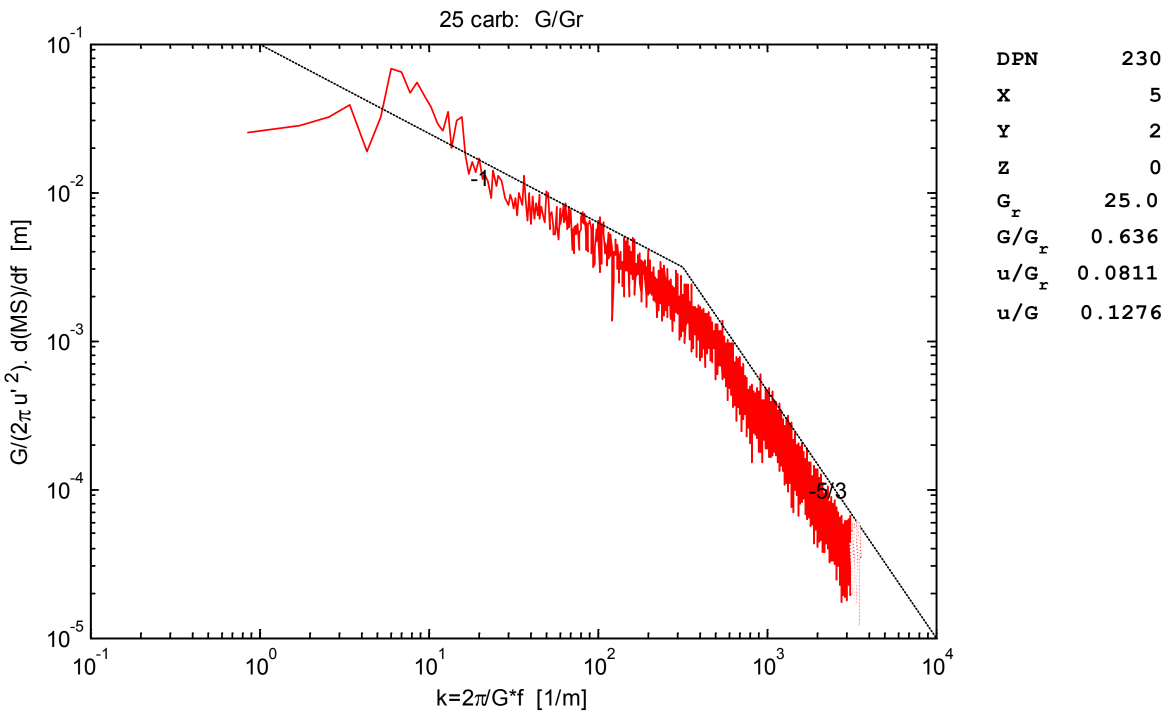

Figure 11 - Turbulence spectrum at Y=2mm, Gr=25m/s, carborundum trip

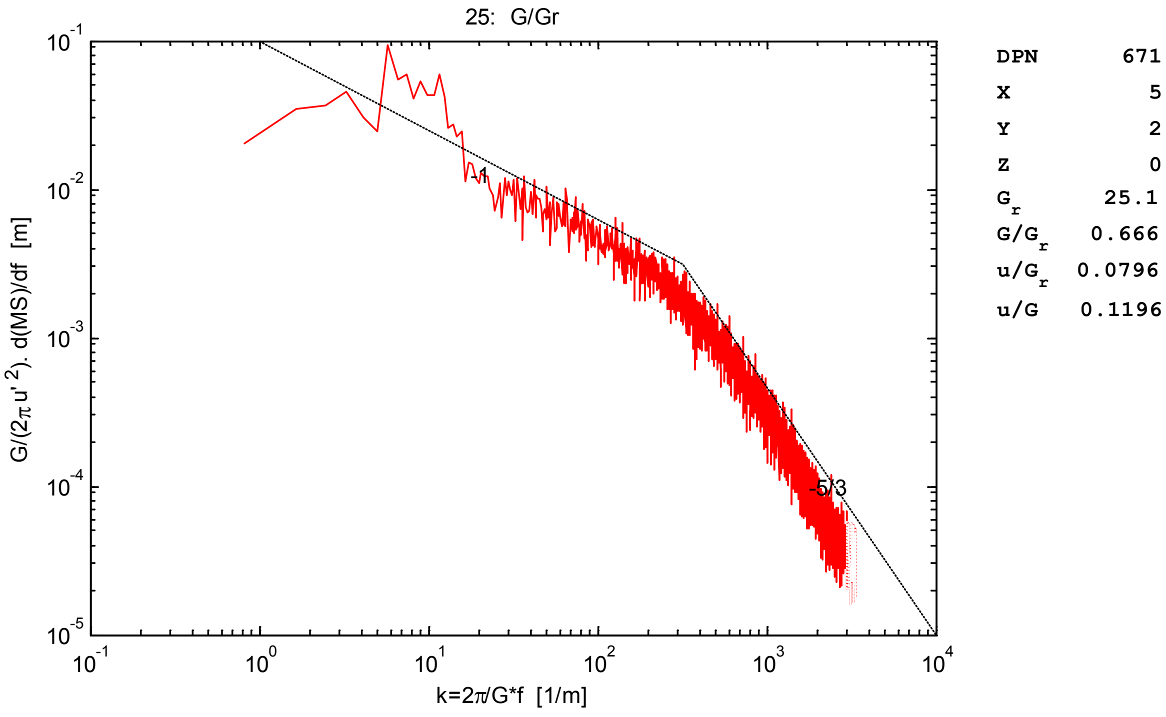

Figure 12 - Turbulence spectrum at Y=2mm, Gr=25m/s, zigzag trip

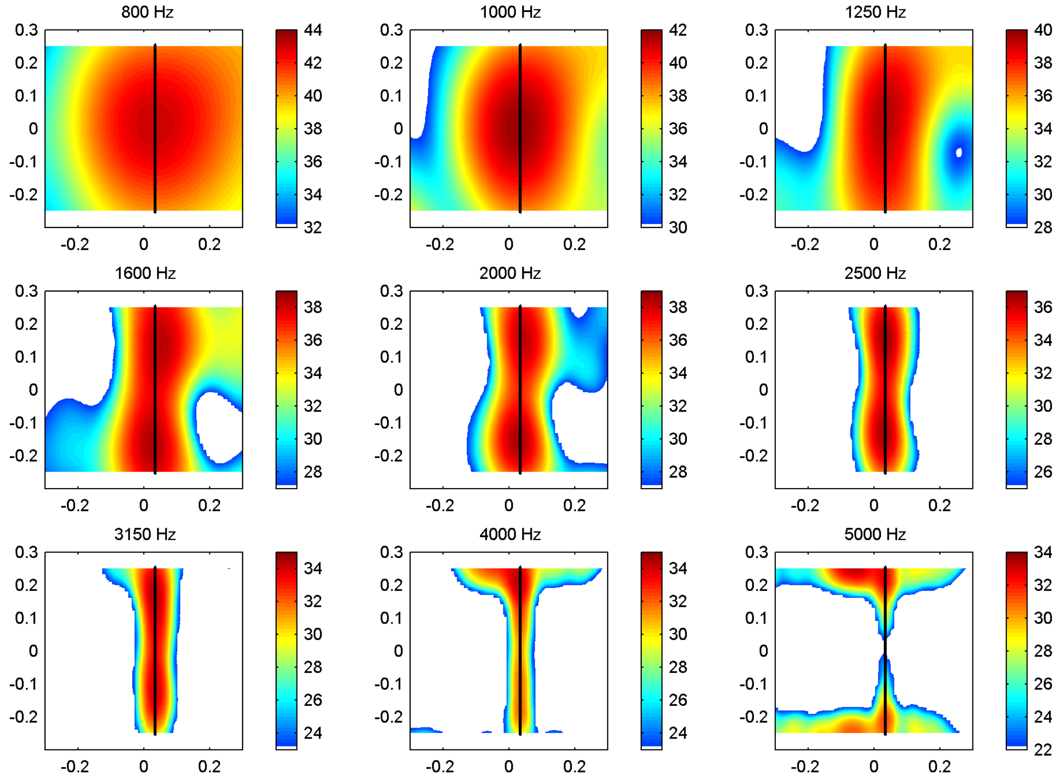

Figure 13 - Acoustic source maps for flat plate with carborundum trip at 20 m/s

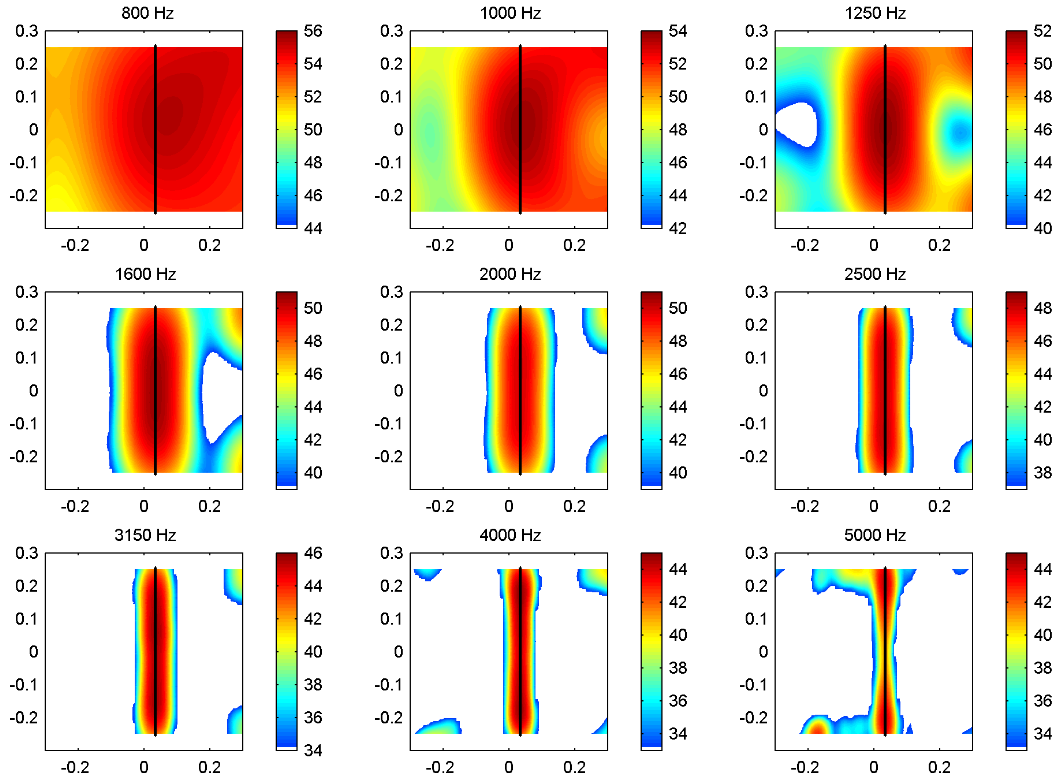

Figure 14 - Acoustic source maps for flat plate with carborundum trip at 35 m/s

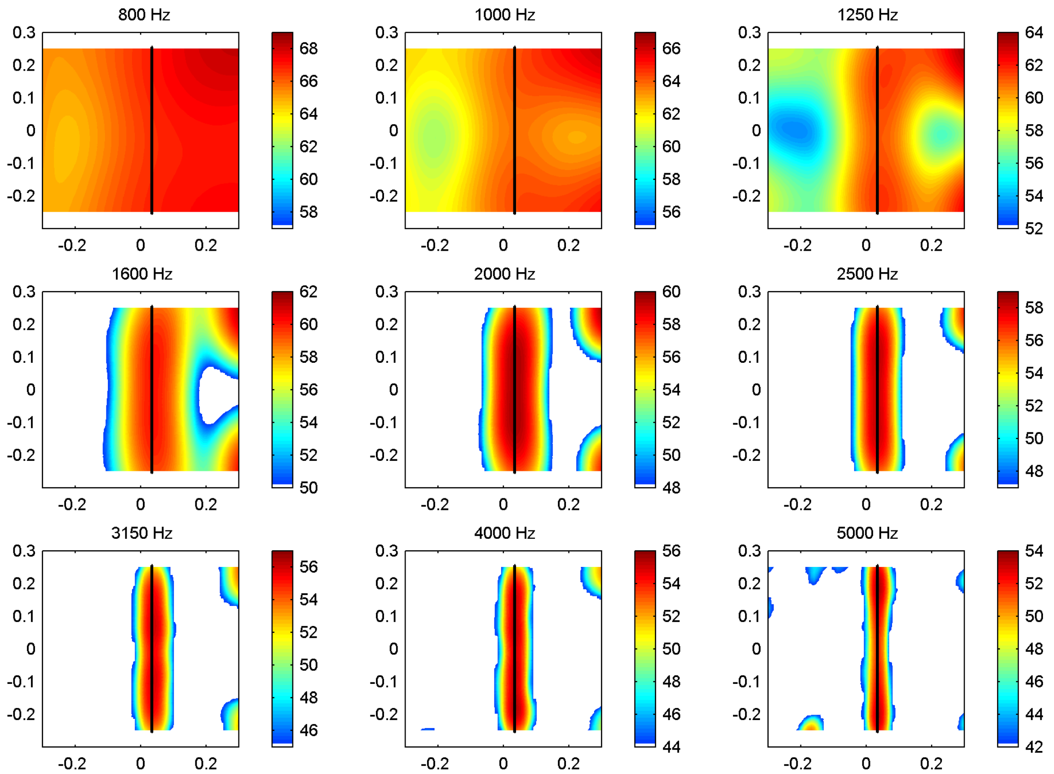

Figure 15 - Acoustic source maps for flat plate with carborundum trip at 55 m/s

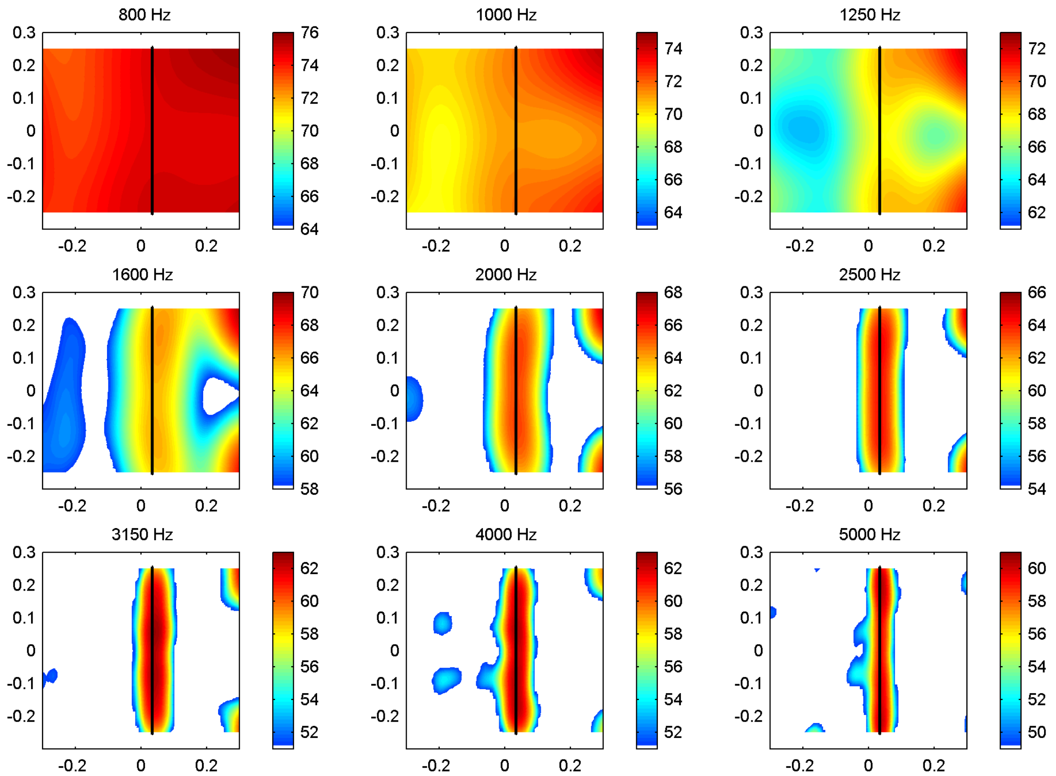

Figure 16 - Acoustic source maps for flat plate with carborundum trip at 75 m/s

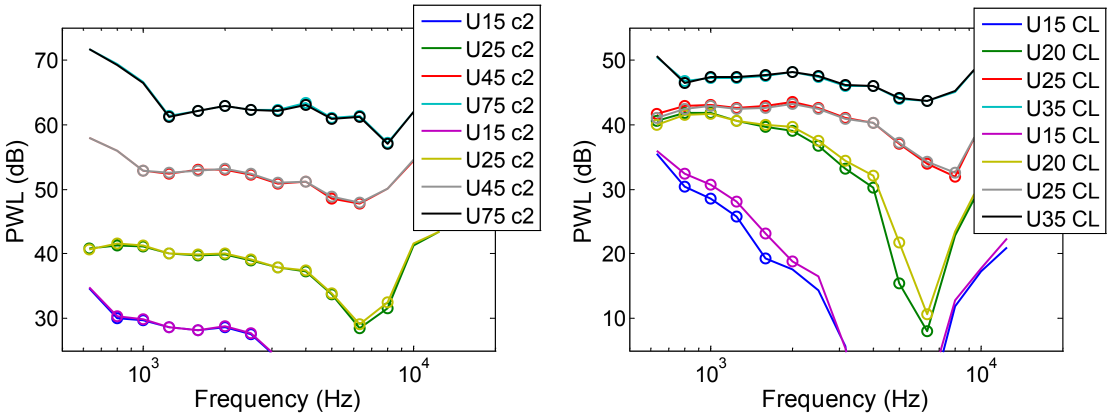

Figure 17 - Repeatability of trailing edge noise spectra for carborundum trip (left) and clean plate (right) at different wind speeds

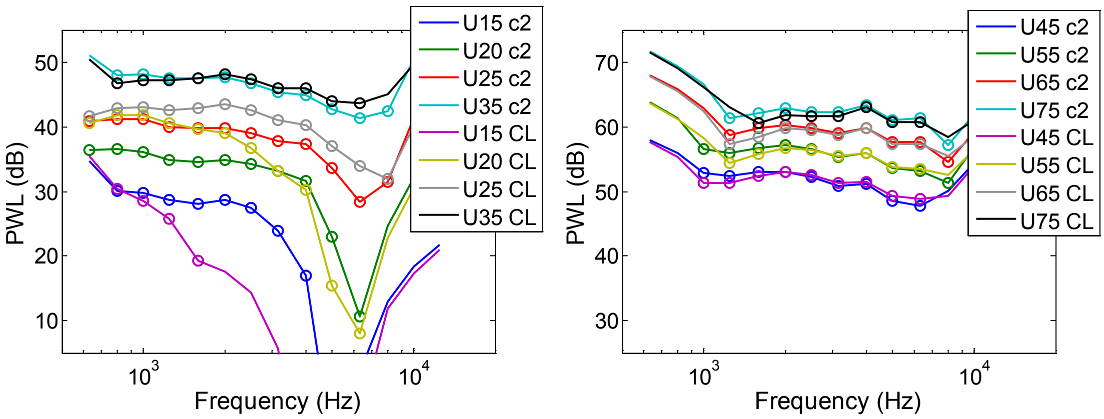

Figure 18 - Comparison between trailing edge noise spectra for carborundum trip and clean plate at low (left) and high (right) wind speeds

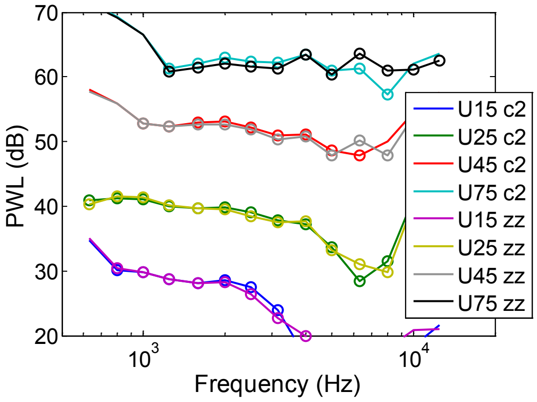

Figure 19 - Comparison between trailing edge noise spectra for carborundum vs zigzag tape

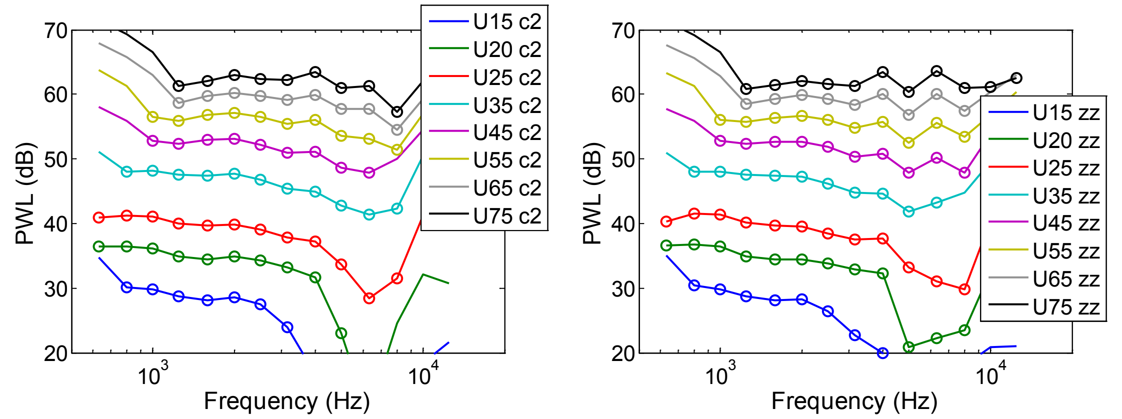

Figure 20 - Trailing edge noise spectra as a function of wind speed for carborundum (left) and zigzag tape (right)

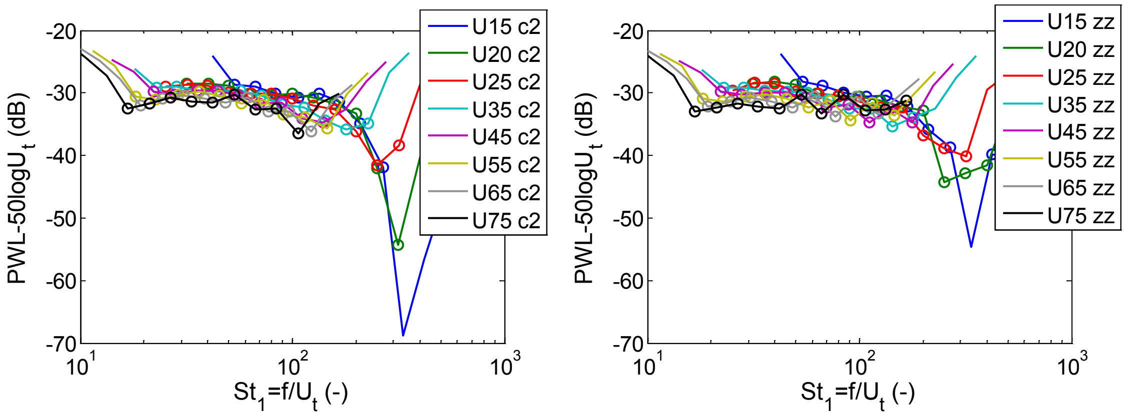

Figure 21 - Normalized trailing edge noise spectra as a function of wind speed for carborundum (left) and zigzag tape (right). A constant length scale is used for normalization

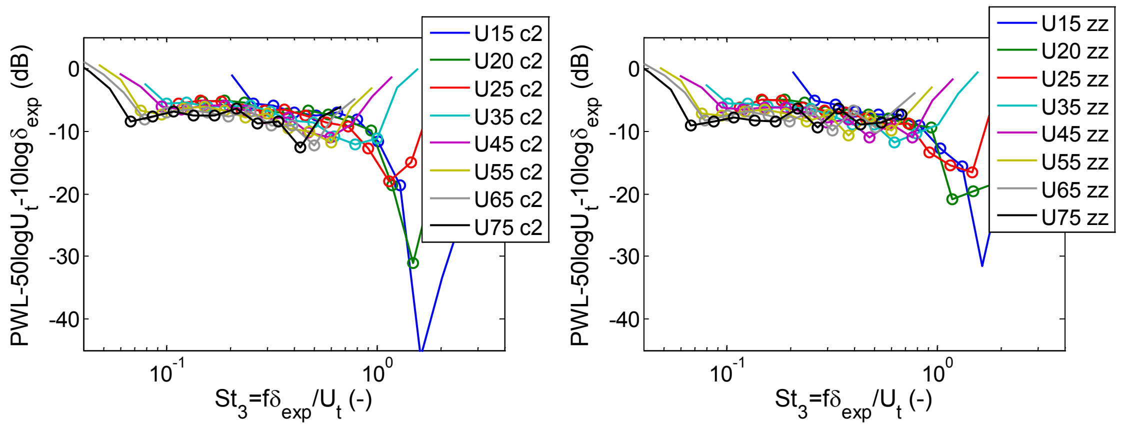

Figure 22 - Normalized trailing edge noise spectra as a function of wind speed for carborundum (left) and zigzag tape (right). The displacement thickness δ_{exp} is used for normalization

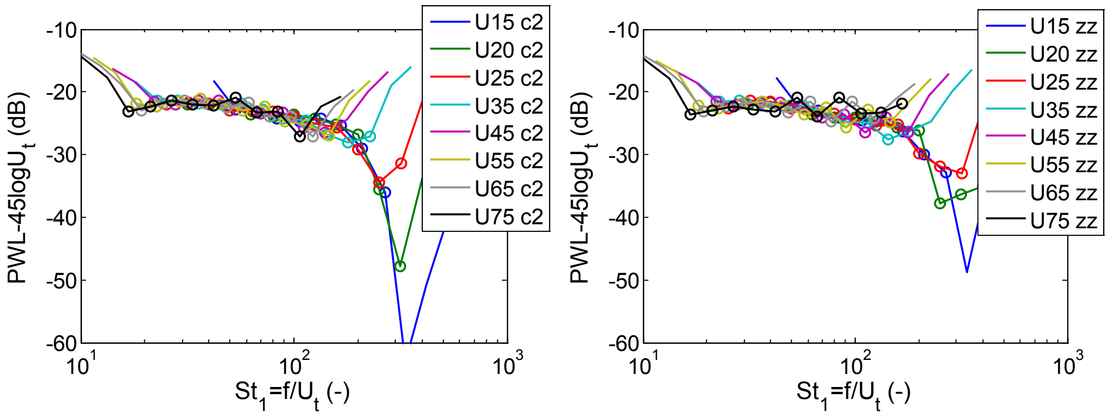

Figure 23 - Normalized trailing edge noise spectra (using a speed power of 4.5 instead of 5) as a function of wind speed for carborundum (left) and zigzag tape (right). A constant length scale is used for normalization

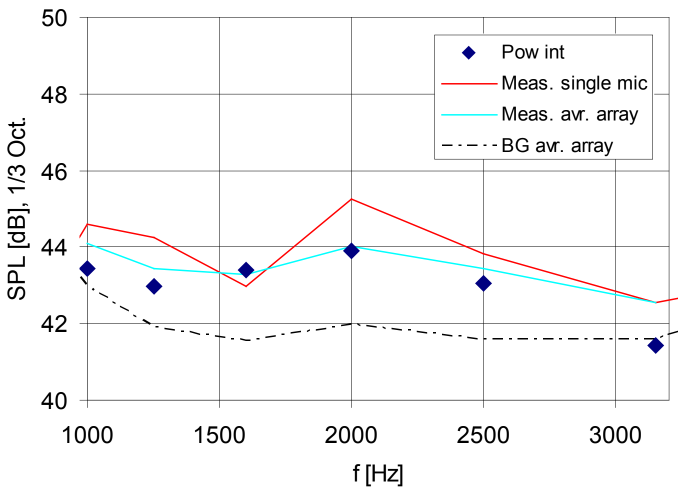

Figure 24 - Comparison spectrum based on a single microphone measurement, averaged spectrum over the microphone array and the power integrated result, clean configuration, U_t=25m/s

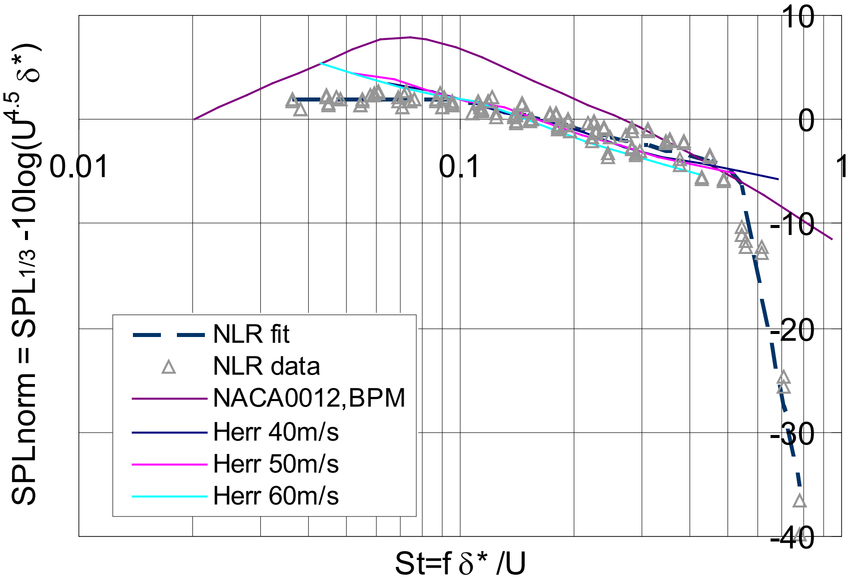

Figure 25 - Normalized TE spectra, comparison of data acquired Herr, NACA0012 BPM[14] prediction and NLR data (carborundum trip, U=15m/s, 20m/s, 25m/s, 35m/s, 45m/s, 55m/s, 65m/s and 75m/s)